Table 2. Frequency of XMRV-Infected Prostatic Cells Determined by FISH

Patient	*RNASEL* Genotype[a]	Number of Cells Counted[b]	Number of FISH-Positive Cells (%)	XMRV FISH[c]	XMRV *gag* RT-PCR
VP 88	QQ	408	5 (1.23)	++	+
VP 31	QQ	526	6 (1.14)	++	−
VP 42	QQ	530	6 (1.13)	++	+
VP 62	QQ	904	10 (1.11)	++	+
VP 29	QQ	659	7 (1.06)	++	+
VP 79	QQ	464	2 (0.43)	+	+
VP 10	QQ	872	1 (0.12)	+/−	−
VP 35	QQ	849	1 (0.12)	+/−	+
VP 90	QQ	843	1 (0.12)	+/−	+
VP 45	RQ	987	0 (0)	−	−
VP 46	RQ	794	0 (0)	−	−
VP 30	RR	661	1 (0.15)	+/−	−
VP 50	RR	787	1 (0.13)	+/−	−
VP 51	RR	842	0 (0)	−	−

[a]*RNASEL* genotypes are as follows: QQ, homozygous R462Q variant; RQ, heterozygous; RR, homozygous wild-type.
[b]*All types of prostatic cells are included.*
[c]+/− = 0.1%–0.2%; + = 0.2%–1%; ++ = >1%.
DOI: 10.1371/journal.ppat.0020025.t002

of humans with a xenotropic MuLV-like agent. Although our efforts to clone the sites of XMRV integration into the host genome have been limited by the small amounts of prostate tissue available for this purpose, our work to clone such sites is ongoing and will provide an important additional piece of evidence for XMRV infection in humans.

The XMRV sequence is not found in human genomic DNA, and none of the human endogenous retroviruses, including the only known gammaretrovirus-like human endogenous sequences (*hERVs E and T*) [70], bare any significant similarity to the XMRV genome. This indicates that XMRV must have been acquired exogenously by infection in positive subjects. From what reservoir and by what route such infections were acquired is unknown. It seems unlikely that direct contact with feral mice could explain the observed distribution of infection in our cohort, since there is no reason to believe that rodent exposure would vary according to *RNASEL* genotype. It is possible that infection is more widespread than indicated by the present studies, especially if, as seems likely, individuals with the wild-type RNase L clear infection more promptly than those with the QQ genotype. But if so, a cross-species transfer model of XMRV infection would require improbably high levels of rodent exposure for a developed society like our own. Thus, although the viral sequence suggests that the ultimate reservoir of XMRV is probably the rodent, the proximate source of the infection seems unlikely to be mice or rats. Provisionally, we favor the notion that the XMRV infections we have documented were acquired from other humans, i.e., that XMRV may have been resident in the human population for some time. This speculation will, however, require direct epidemiologic validation. It also remains to be determined if RNase L R462Q homozygotes are more sensitive to the acquisition of infection, or are simply less likely to clear infection once acquired. This is an important issue, since if the latter model is correct, it would imply that in younger humans, XMRV prevalence may be higher than what is observed in our prostate cancer cohort (mean age 58.7 y). We are currently developing serologic assays for use in population-based studies that should shed light on these matters.

While presented work documents a clear link of XMRV infection to RNase L deficiency, we emphasize that the data we have accumulated does not mandate any etiological link to prostate cancer. Furthermore, our finding that XMRV infection is targeted to stromal cells and not to carcinoma cells and the fact that the XMRV genome harbors no host-derived oncogenes rule out two classical models for retroviral oncogenesis: direct introduction of a dominantly acting oncogene and insertional activation of such a gene. However, more indirect contributions of the virus to the tumor can certainly be envisioned. Recent work has shown that stromal cells have an active role in directly promoting tumorigenesis of adjacent epithelial cells by producing various cytokines and growth factors that serve as proliferative signals [71] or indirectly by modifying the tumor microenvironment by promotion of angiogenesis or recruitment of inflammatory mediators leading to oxidative stress [72]. In particular, cancer-associated fibroblasts stimulate growth of human prostatic epithelial cells and alter their histology in vivo [73]. It is conceivable that XMRV-infected prostatic stromal cells could produce and secrete growth factors, cytokines or other factors that stimulate cell proliferation or promote oxidative stress in surrounding epithelia. Such a paracrine mechanism could still function quite efficiently even with the relatively small number of XMRV-infected cells that characterize the lesion.

Finally, we note that the identification of an exogenous infection such as XMRV could help explain why not all genetic studies have consistently identified RNase L as a prostate cancer susceptibility factor. If such an infection were linked, however indirectly, to prostate cancer risk, and if the prevalence of infection is not uniform in different populations, populations with low XMRV prevalence might be expected to show no association of *RNASEL* lesions to prostate cancer.

Clearly, resolution of these issues will require much further investigation. We need to determine the prevalence of XMRV infection in the general population, understand its routes of transmission and tissue tropism, explore its associations with pre-maligant and other prostatic conditions, and define the biochemical interactions of the virus with the 2–5A/RNase L system. The availability of molecular clones, infectious virus stocks, and susceptible cell culture systems should greatly enhance our ability to probe these and other questions in the near future.

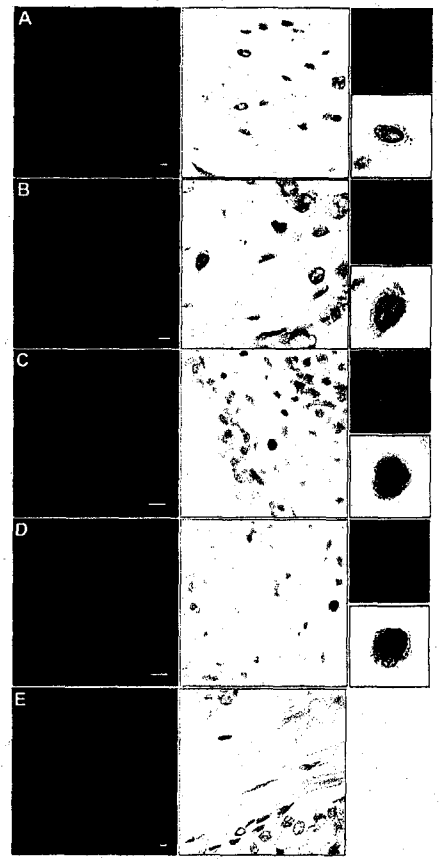

Figure 9. Detection of XMRV Protein in Prostatic Tissues Using *Immunostaining*

Prostatic tumor tissue sections from QQ cases VP62 (A and B) and VP88 (C and D), as well as an RR case VP51 (E) were stained, then visualized by immunofluorescence (left) or bright field (middle) using a monoclonal antibody to SFFV Gag protein. Nuclei are counterstained with hematoxylin. Enlarged images corresponding to the positive cells are shown on the right. Scale bars are 5 μm in (A), (B), and (E) and 10 μm in (C) and (D).
DOI: 10.1371/journal.ppat.0020025.g009

Materials and Methods

Genotyping of patients, and prostate tissue processing. All human samples used in this study were obtained according to protocols approved by the Cleveland Clinic's Institutional Review Board. Age, clinical parameters, and geographical locations of XMRV-positive prostate cancer cases are provided in Table S5. Men scheduled to undergo prostatectomies at the Cleveland Clinic were genotyped for the R462Q (1385C->A) *RNASEL* variant using a premade TAQMAN genotyping assay (Applied Biosystems, Foster City, California, United States; Assay c__935591__1) on DNA isolated from peripheral blood mononuclear cells. Five nanograms of genomic DNA were assayed according to the manufacturer's instructions, and analyzed on an Applied Biosystems 7900HT Sequence Detection System instrument. Immediately after prostatectomies, tissue cores were taken from both the transitional zone (the site of benign prostatic hyperplasia, BPH) and the peripheral zone (where cancer generally occurs), snap-frozen in liquid nitrogen, and then stored at −80 °C. Remaining prostate tissue was fixed in 10% neutral buffered formalin, processed, and embedded in paraffin for later histological analyses. Frozen tissue cores were transferred from dry ice immediately to TRIZOL reagent (Invitrogen, Carlsbad, California, United States), homogenized with a power homogenizer or manually using a scalpel followed by a syringe, and total RNA was isolated according to the manufacturer's instructions. The prostate tissue RNA was then subjected to RNase-free DNase I (Ambion, Austin, Texas, United States) digestion for 30 min at 37 °C. The sample was then extracted with phenol and the RNA was precipitated with isopropanol overnight at −20 °C followed by centrifugation at 12,000 g for 30 min at 4 °C. Poly-A RNA was isolated from the DNase digested total RNA using the Oligotex mRNA Midi Kit (Qiagen USA, Valencia, California, United States) as instructed by the manufacturer. The poly-A RNA concentration was measured using the RIBOgreen quantitation kit (Molecular Probes, Invitrogen), and the samples were stored at −80 °C.

Microarray screening. Virochip microarrays used in this study were identical to those previously described [20–22]. Prostate tumor RNA samples were amplified and labeled using a modified Round A/B random PCR method and hybridized to the Virochip microarrays as reported previously (Protocol S1 in [21]). Microarrays were scanned with an Axon 4000B scanner (Axon Instruments, Union City, California, United States) and gridded using the bundled GenePix 3.0 software. Microarray data have been submitted to the NCBI GEO database (GSE3607). Hybridization patterns were interpreted using E-Predict as previously described [22] (Table S1). To make Figure 1, background-subtracted hybridization intensities of all retroviral oligonucleotides (205) were used to cluster samples and the oligonucleotides. Average linkage hierarchical clustering with Pearson correlation as the similarity metric was carried out using Cluster (version 2.0) [74]. Cluster images were generated using Java TreeView (version 1.0.8) [75].

Genome cloning and sequencing. Amplified and labeled cDNA from the VP35 tumor sample was hybridized to a hand-spotted microarray containing several retroviral oligonucleotides, which had high hybridization intensity on the Virochip during the initial microarray screening. Nucleic acid hybridizing to two of the oligonucleotides (9628654__317__rc derived from MTCR: TTC GCT TTA TCT GAG TAC CAT GTG TTC TTG GCC GTG AGC CGG GGC CCA GGT GCT CGA CCA CAG ATA TCC T; and 9626955__16__rc derived from SFFV: TCG GAT GCA ATC AGC AAG AGG CTT TAT TGC GAA CAC GGG TAC CCG GGC GAC TCA GTC TGT CGG AGG ACT G) was then individually eluted off the surface of the spots and amplified by PCR with Round B primers. Preparation of the hand-spotted array, hybridization, probe recovery, and PCR amplification of the recovered material were carried out according to Protocol S1. The recovered amplified DNA samples were then cloned into pCR2.1-TOPO TA vector (Invitrogen), and the resulting libraries were screened by colony hybridization with the corresponding above oligonucleotides as probes. Hybridizations were carried out using Rapid-Hyb buffer (Amersham, Piscataway, New Jersey, United States) according to the manufacturer's protocol at 50 °C for 4 h. Eight positive clones were sequenced, of which two (one from each library; clones K1 and K2R1 in Figure 2A) were viral and had 94–95% nt identity to MTCR.

To sequence the remainder of the VP35 genome as well as the entire genome from the VP42 tumor, we amplified fragments of the genome by PCR using either amplified (Round B) or unamplified

(Round A) cDNA prepared for original Virochip screening. This was accomplished first using a combination of primers derived from the sequence of MTCR and earlier recovered clones of XMRV. The two overlapping fragments from VP62 were amplified by PCR from cDNA generated by priming poly-A RNA with random hexamers. All PCR primers are listed in Table S2. The amplified fragments were cloned into pCR2.1-TOPO TA vector (Invitrogen) and sequenced using M13 sequencing primers. Genome assembly was carried out using CONSED version 13.84 for Linux [76].

PCR. Screening of tumor samples by *gag* nested RT-PCR was carried out according to Protocol S2. PCR fragments in all positive cases were gel-purified using QIAEX II gel extraction kit (Qiagen), cloned into pCR2.1-TOPO TA vector (Invitrogen), and sequenced using M13 sequencing primers.

Pol PCR was carried out using amplified cDNA (Round B material) as the template.

Sequence of the primers used for amplification (2670F, 3870R, 3810F, and 5190R) is listed in Table S2. Amplified products were gel-purified using QIAEX II gel extraction kit (Qiagen), and purified products were directly used for sequencing.

Phylogenetic analyses. Xenotropic mERV Chromosome 1, xenotropic mERV Chromosome 4, and xenotropic mERV Chromosome 9 were chosen by BLAST querying the NCBI nr database with the complete XMRV genomes and selecting the most similar full-length proviral sequences, all of which happened to have xenotropic envelopes (Figure S2C). Polytropic mERV Chromosome 7 and polytropic mERV Chromosome 11 were chosen by selecting NCBI nr full-length proviral sequences with envelopes most similar to a prototype polytropic clone MX27 [77]. Similarly, modified polytropic mERV Chromosome 7 and modified polytropic mERV Chromosome 12 were selected on the basis of similarity to a prototype-modified polytropic clone MX33 [77]. U3 analysis was performed using previously described reference sequences: Mcv18, Mcv3, Mxv2, Mcv11, Mxv11, and HEMV18 [49]; CWM-T-15, CWM-T-15-4, CWM-T-25a, and CWM-T-25b [48].

To generate the neighbor-joining tree of complete genomic sequences (Figure 3), the sequences were first manually edited to make all genomes the same length, i.e., R to R. The edited sequences were then aligned with ClustalX version 1.82 for Linux [78,79] using default settings. The tree was generated based on positions without gaps only; Kimura correction for multiple base substitutions [80] and bootstrapping with $n = 1000$ were also used.

All other trees were generated as above, except sequences were first trimmed to the same length, gaps were included, and Kimura correction was not used, as using these parameters did not have any significant effect on the trees.

Antibodies. Monoclonal antibody to SFFV Gag protein was produced from R187 cells ([65]; ATCC: CRL-1912) grown in DMEM (Media Core, Cleveland Clinic Foundation, Cleveland, Ohio, United States) with 10% ultra-low IgG FBS (Invitrogen) until confluent. Conditioned media was collected every three days from confluent cultures. Five ml of conditioned media per preparation was centrifuged at 168 × g for 5 min at 4 °C. Supernatant was filtered through a 0.22-μm syringe filter unit (Millipore, Billerica, Massachusetts, United States) and concentrated 16-fold in an Amicon ultrafiltration unit with a 100-kDa molecular weight cutoff membrane (Millipore). Sodium azide was added to a final concentration of 0.02%. Concomitant XMRV FISH/cytokeratin immunofluorescence was performed using a mouse anti-cytokeratin AE1/AE3 (20:1 mixture) monoclonal antibody (Chemicon International, Temecula, California, United States) capable of recognizing normal and neoplastic cells of epithelial origin.

FISH. The XMRV-35 FISH probe cocktail was generated using both 2.15-kb and 1.84-kb segments of the viral genome obtained by PCR with forward primer-2345, 5′ ACC CCT AAG TGA CAA GTC TG 3′ with reverse primer-4495, 5′ CTG GAC AGT GAA TTA TAC TA 3′ and forward primer-4915, 5′ AAA TTG GGG CAG GGG TGC GA 3′ with reverse primer-6755, 5′ TTG GAG TAA GTA CCT AGG AC 3′, both cloned into pGEM-T (Promega, Madison, Wisconsin, United States). The recombinant vectors were digested with *EcoR*I to release the viral cDNA fragments, which were purified after gel electrophoresis (Qiagen). The purified viral cDNA inserts were used in nick translation reactions to produce SpectrumGreen dUTP fluorescently labeled probe according to manufacturer's instructions (Vysis Inc., Des Plaines, Illinois, United States). Freshly baked slides of prostatic tissues or tissue microarray arrays with ~4-μm thick tissue sections were deparaffinized, rehydrated, and subjected to Target Retrieval (Dako, Glostrup, Denmark) for 40 min at 95 °C. Slides were cooled to room temperature and rinsed in H_2O. Proteinase K (Dako) at 1:5000 in Tris-HCl (pH 7.4) was applied directly to slides for 10 min at room temperature. Adjacent tissue sections were also probed with SpectrumGreen dUTP fluorescently labeled KSHV-8 DNA (nts 85820–92789) as a negative control or, as a positive control with SpectrumGreen and SpectrumOrange labeled TelVysion DNA Probe cocktail (Vysis), specific for subtelomeric regions of the P and Q arms of human Chromosome 1 as a positive control to ensure the tissue was completely accessible to FISH. FISH slides were examined using a Leica DMR microscope (Leica Micro-Systems, Heidelberg, Germany), equipped with a Retiga EX CCD camera (Q-Imaging,Vancouver, British Columbia, Canada). FISH images were captured using a Leica TCS SP2 laser scanning confocal with a 63× oil objective numerical aperature 1.4 (Leica Micro-Systems) microscope. XMRV nucleic acids were visualized using maximum intensity projections of optical slices acquired using a 488-nm argon-laser (emission at 500–550 nm). TelVysion DNA Probes were visualized using maximum intensity projections of optical slices acquired using a 488-nm argonlaser (emission at 500–550 nm) and 568-nm krypton-argon-laser (emission at 575–680 nm). DAPI was visualized using maximum intensity projections of optical slices acquired using a 364-nm UV-laser (emission at 400–500 nm). Slides were subsequently washed in 2× SSC (0.3 M sodium chloride and 0.03 M sodium citrate, [pH 7.0]) to remove coverslips, and H&E stained for morphological evaluation.

IHC. IHC on human tissues was performed on a Benchmark Ventana Autostainer (Ventana Medical Systems, Tucson, Arizona, United States). Unstained, formalin-fixed, paraffin-embedded prostate sections were placed on electrostatically charged slides and deparaffinized followed by a mild cell conditioning achieved through the use of Cell Conditioner #2 (Ventana Medical Systems). The concentrated R187 monoclonal antibody against SFFV p50 Gag was dispensed manually onto the sections at 10 μg per ml and allowed to incubate for 32 min at 37 °C. Endogenous biotin was blocked in sections using the Endogenous Biotin Blocking Kit (Ventana Medical Systems). Sections were washed, and biotinylated ImmunoPure Goat Anti-Rat IgG (Pierce Biotechnology, Rockford, Illinois, United States) was applied at a concentration of 4.8 μg per ml for 8 min. To detect Gag protein localization, the Ventana Enhanced Alkaline Phosphatase Red Detection Kit (Ventana Medical Systems) was used. Sections were briefly washed in distilled water and counterstained with Hematoxylin II (Ventana Medical Systems) for approximately 6 min. Sections were washed, dehydrated in graded alcohols, incubated in xylene for 5 min, and coverslips were added with Cytoseal (Microm International, Walldorf, Germany). Negative controls were performed as above except without the addition of the R187 monoclonal antibody.

Concomitant XMRV FISH/cytokeratin IHC was performed on slides of prostate tissue from patient VP62. First, sections were immunostained for cytokeratin AE1/AE3 using the Alexa Fluor 594 Tyramide Signal Amplification Kit (Molecular Probes, Invitrogen). Briefly, unstained, formalin-fixed, paraffin-embedded sections cut at ~4 μm were placed on electrostatically charged slides, baked at 65 °C for at least 4 h, deparaffinized in xylene, and rehydrated through decreasing alcohol concentrations. Slides were incubated in Protease II (Ventana Medical Systems) for 3 min at room temperature and washed in phosphate-buffered saline (PBS) in peroxidase quenching buffer (PBS + 3% H_2O_2) for 60 min at room temperature, then incubated with 1% blocking reagent (10 mg/ml BSA in PBS) for 60 min at room temperature. The slides were incubated with cytokeratin AE1/AE3 antibody diluted in 1% blocking reagent for 60 min at room temperature and rinsed 3× times in PBS. Goat anti-mouse IgG-horseradish peroxidase (Molecular Probes, Invitrogen) was added and incubated for 60 min at room temperature. The slides were rinsed 3× in PBS. The tyramide solution was added to the slides for 10 min at room temperature and the slides were rinsed 3× in PBS. Slides were then placed in Target Retrieval solution (Dako) for 40 min at 95 °C. FISH for XMRV was performed as described above except in the absence of proteinase K treatment. After FISH, the slides were mounted with Vectashield Mounting Medium plus DAPI (Vector Labs, Burlingame, California, United States) and examined using fluorescence microscopy. Immunofluorescence images were captured using a Texas red filter with a Leica DMR microscope (Leica Micro-Systems), equipped with a Retiga EX CCD camera (QImaging).

Supporting Information

Figure S1. Complete Nucleotide Sequence of XMRV VP35

Numbers to the left indicate nt coordinates relative to the first nt. Predicted open reading frames for Gag, Gag-Pro-Pol, and Env polyproteins are shown below the corresponding nt. Characteristic 24-nt deletion in the 5′ *gag* leader is indicated with a triangle. Other genome features as well as primers used in the nested *gag* RT-PCR are shown as arrows.

Found at DOI: 10.1371/journal.ppat.0020025.sg001 (558 KB PDF).

Figure S2. Phylogenetic Analysis of XMRV Based on Predicted Gag, Pro-Pol, and Env Polyproteins

Predicted Gag (A), Pro-Pol (B), and Env (C) sequences of XMRV VP35, VP42, and VP62 (red) as well as the correspondihg sequences from MTCR; MuLVs DG-75, MCF1233, Akv, Moloney, Friend, and Rauscher; feline leukemia virus (FLV); koala retrovirus (KoRV); gibbon ape leukemia virus (GALV), and a set of representative non-ecotropic proviruses (mERVs) were aligned using ClustalX. The resulting alignments were used to generate unrooted neighbor-joining trees (see Materials and Methods). Sequences are labeled as xenotropic (X), polytropic (P), modified polytropic (Pm), or ecotropic (E).

Found at DOI: 10.1371/journal.ppat.0020025.sg002 (186 KB EPS).

Figure S3. Comparison of XMRV U3 Region to Representative Non-Ecotropic Sequences

(A) Multiple sequence alignment of U3 sequences from XMRV VP35, VP42, and VP62; MuLVs NZB-9-1 and NFS-Th-1; and from representative non-ecotropic proviruses [37,48,49]. The sequences were aligned using ClustalX (see Materials and Methods). Only sequences most similar to XMRV are shown. Glucocorticoid response element (GRE), and TATA and CAT boxes are indicated by lines. Direct repeat regions (boxed) are numbered according to the existing convention [37,49]. Triangle indicates a 190 nt insertion in polytropic proviruses [37]. XMRV-specific AG dinucleotide insertion is shown in red. Dots denote nt identical to those from XMRV, and deleted nt appear as spaces.

(B) Phylogenetic tree based on U3 nt sequences. Multiple sequence alignment from (A) was used to generate an unrooted neighbor-joining tree (see Materials and Methods). Bootstrap values ($n = 1000$ trials) are shown as percentages. U3 sequences from XMRV are shown in red.

Found at DOI: 10.1371/journal.ppat.0020025.sg003 (188 KB EPS).

Protocol S1. Probe Recovery from Hand-Spotted Microarrays by "Scratching"

Found at DOI: 10.1371/journal.ppat.0020025.sd001 (83 KB PDF).

Protocol S2. XMRV *gag* Nested RT-PCR

Found at DOI: 10.1371/journal.ppat.0020025.sd002 (172 KB PDF).

Table S1. Computational Viral Species Predictions Using E-Predict for the Virochip Microarrays Shown in Figure 1

Found at DOI: 10.1371/journal.ppat.0020025.st001 (48 KB DOC).

Table S2. PCR Primers Used for Sequencing of XMRV Genomes

Found at DOI: 10.1371/journal.ppat.0020025.st002 (45 KB DOC).

Table S3. Age, Clinical Parameters, and Geographical Locations of XMRV-Positive Prostate Cancer Cases

Found at DOI: 10.1371/journal.ppat.0020025.st003 (39 KB DOC).

Video S1. Confocal Optical Image Planes of a Representative XMRV FISH Positive Cell

Optical image planes (0.5 μm step-size) of the XMRV FISH positive cell from Figure 1A acquired using a Leica TCS SP2 laser scanning spectral confocal microscope (Leica, Heidelberg, Germany) were reconstructed into a 3D volume set using Volocity 3.5 (Improvision, Lexington, Massachusetts, United States). Using Volocity's movie sequence editor, each volume was rotated along horizontal and vertical axes, adjusting nuclei stained DAPI (blue) channel brightness to visualize underlying XMRV FISH (green) nucleic acid signal. The resulting image frames were exported as a movie sequence. Underlying grid represents glass slide to which tissue was placed for FISH analysis. Each square unit within grid represents 4 μm in height and width.

Found at DOI: 10.1371/journal.ppat.0020025.sv001 (237 KB WMV).

Accession Numbers

Accession numbers from Gen Bank (http://www.ncbi.nlm.nih.gov/Genbank) are: AKV MuLV (J01998), feline leukemia virus (NC_001940), Friend MuLV (NC_001372), gibbon ape leukemia virus (NC_001885), koala retrovirus (AF151794), modified polytropic mERV Chromosome 7 (AC127565; nt 64,555–72,720), modified polytropic mERV Chromosome 12 (AC155658; nt 85,452–93,817), Moloney MuLV (NC_001501), MTCR (NC_001702MuLV DG-75 (AF221065); MuLV MCF 1233 (U13766), MuLV NCI-417 (AAC97875), MuLV NZB-9-1 (K02730), polytropic mERV Chromosome 7 (AC167978; nt 57,455–65,805), polytropic mERV Chromosome 11 (168–229,176,580), polytropic clone MX27 (M17327), Rauscher MuLV (NC_001819), xenotropic mERV Chromosome 1 (AC083892, nt 158,240–166,448), xenotropic mERV Chromosome 4 (AL627077; nt 146,400–154,635), xenotropic mERV Chromosome 9 (AC121813; nt 37,520–45,770), XMRV VP35 (DQ241301), XMRV VP42 (DQ241302), and XMRV VP 62 (DQ399707).

Acknowledgments

We thank Silvi Rouskin, Shoshannah Beck, James Pettay, and Jayashree Paranjape for expert technical assistance; Sanggu Kim and Samson A. Chow for technical advice; Earl Poptic for production and purification of monoclonal antibodies to Gag; Stephen T. Koury for advice; and Judith A. Drazba and Amit Vasanji for assistance with confocal imaging.

Author contributions. AU, RJM, NF, DG, RHS, and JLD conceived and designed the experiments. AU, RJM, NF, SJP, KM, CMG, and RRT performed the experiments. AU, RJM, NF, SJP, GC, EAK, KM, CMG, RRT, DG, RHS, and JLD analyzed the data. AU, RJM, NF, SJP, GC, EAK, DG, RHS, and JLD contributed reagents/materials/analysis tools. AU, RJM, NF, DG, RHS, and JLD wrote the paper.

Funding. This investigation was supported by Genentech Graduate Fellowship and a grant from the Sandler Family Supporting Foundation (AU), grants from Doris Duke Charitable Foundation (JLD and DG) and the David and Lucille Packard Foundation (JLD), Howard Hughes Medical Institute (JLD and DG), by NIH/NCI grants (to RHS and GC), and a Molecular Medicine Fellowship from Cleveland State University and the Cleveland Clinic Foundation (RJM).

Competing interests. The authors have declared that no competing interests exist.

References

1. Kerr IM, Brown RE (1978) pppA2′p5′A2′p5′A: An inhibitor of protein synthesis synthesized with an enzyme fraction from interferon-treated cells. Proc Natl Acad Sci U S A 75: 256–260.
2. Zhou A, Hassel BA, Silverman RH (1993) Expression cloning of 2–5A-dependent RNAase: A uniquely regulated mediator of interferon action. Cell 72: 753–765.
3. Dong B, Silverman RH (1995) 2–5A-dependent RNase molecules dimerize during activation by 2–5A. J Biol Chem 270: 4133–4137.
4. Zhou A, Paranjape J, Brown TL, Nie H, Naik S, et al. (1997) Interferon action and apoptosis are defective in mice devoid of 2′,5′-oligoadenylate-dependent RNase L. EMBO J 16: 6355–6363.
5. Flodstrom-Tullberg M, Hultcrantz M, Stotland A, Maday A, Tsai D, et al. (2005) RNase L and double-stranded RNA-dependent protein kinase exert complementary roles in islet cell defense during coxsackievirus infection. J Immunol 174: 1171–1177.
6. Castelli JC, Hassel BA, Wood KA, Li XL, Amemiya K, et al. (1997) A study of the interferon antiviral mechanism: Apoptosis activation by the 2–5A system. J Exp Med 186: 967–972.
7. Li G, Xiang Y, Sabapathy K, Silverman RH (2004) An apoptotic signaling pathway in the interferon antiviral response mediated by RNase L and c-Jun NH2-terminal kinase. J Biol Chem 279: 1123–1131.
8. Malathi K, Paranjape JM, Ganapathi R, Silverman RH (2004) HPC1/RNASEL mediates apoptosis of prostate cancer cells treated with 2′,5′-oligoadenylates, topoisomerase I inhibitors, and tumor necrosis factor-related apoptosis-inducing ligand. Cancer Res 64: 9144–9151.
9. Xiang Y, Wang Z, Murakami J, Plummer S, Klein EA, et al. (2005) Effects of RNase L mutations associated with prostate cancer on apoptosis induced by 2′,5′-oligoadenylates. Cancer Res 65: 6795–6801.
10. Carpten J, Nupponen N, Isaacs S, Sood R, Robbins C, et al. (2002) Germline mutations in the ribonuclease L gene in families showing linkage with HPC1. Nat Genet 30: 181–184.
11. Casey G, Neville PJ, Plummer SJ, Xiang Y, Krumroy LM, et al. (2002) RNASEL Arg462Gln variant is implicated in up to 13% of prostate cancer cases. Nat Genet 32: 581–583.

12. Rennert H, Bercovich D, Hubert A, Abeliovich D, Rozovsky U, et al. (2002) A novel founder mutation in the RNASEL gene, 471delAAAG, is associated with prostate cancer in Ashkenazi Jews. Am J Hum Genet 71: 981–984.
13. Rokman A, Ikonen T, Seppala EH, Nupponen N, Autio V, et al. (2002) Germline alterations of the RNASEL gene, a candidate HPC1 gene at 1q25, in patients and families with prostate cancer. Am J Hum Genet 70: 1299–1304.
14. Nelson WG, De Marzo AM, Isaacs WB (2003) Prostate cancer. N Engl J Med 349: 366–381.
15. Carter BS, Bova GS, Beaty TH, Steinberg GD, Childs B, et al. (1993) *Hereditary prostate cancer: Epidemiologic and clinical features.* J Urol 150: 797–802.
16. Silverman RH (2003) Implications for RNase L in prostate cancer biology. Biochemistry 42: 1805–1812.
17. Downing SR, Hennessy KT, Abe M, Manola J, George DJ, et al. (2003) Mutations in ribonuclease L gene do not occur at a greater frequency in patients with familial prostate cancer compared with patients with sporadic prostate cancer. Clin Prostate Cancer 2: 177–180.
18. Wiklund F, Jonsson BA, Brookes AJ, Stromqvist L, Adolfsson J, et al. (2004) Genetic analysis of the RNASEL gene in hereditary, familial, and sporadic prostate cancer. Clin Cancer Res 10: 7150–7156.
19. Maier C, Haeusler J, Herkommer K, Vesovic Z, Hoegel J, et al. (2005) Mutation screening and association study of RNASEL as a prostate cancer susceptibility gene. Br J Cancer 92: 1159–1164.
20. Wang D, Coscoy L, Zylberberg M, Avila PC, Boushey HA, et al. (2002) Microarray-based detection and genotyping of viral pathogens. Proc Natl Acad Sci U S A 99: 15687–15692.
21. Wang D, Urisman A, Liu YT, Springer M, Ksiazek TG, et al. (2003) Viral discovery and sequence recovery using DNA microarrays. PLoS Biol 1: e2. DOI: 10.1371/journal.pbio.0000002
22. Urisman A, Fischer KF, Chiu CY, Kistler AL, Beck S, et al. (2005) E-Predict: A computational strategy for species identification based on observed DNA microarray hybridization patterns. Genome Biol 6: R78.
23. Clark SP, Mak TW (1983) Complete nucleotide sequence of an infectious clone of Friend spleen focus-forming provirus: gp55 is an envelope fusion glycoprotein. Proc Natl Acad Sci U S A 80: 5037–5041.
24. Raisch KP, Pizzato M, Sun HY, Takeuchi Y, Cashdollar LW, et al. (2003) Molecular cloning, complete sequence, and biological characterization of a xenotropic murine leukemia virus constitutively released from the human B-lymphoblastoid cell line DG-75. Virology 308: 83–91.
25. Wheeler DL, Church DM, Federhen S, Lash AE, Madden TL, et al. (2003) Database resources of the National Center for Biotechnology. Nucleic Acids Res 31: 28–33.
26. Wills NM, Gesteland RF, Atkins JF (1991) Evidence that a downstream pseudoknot is required for translational read-through of the Moloney murine leukemia virus gag stop codon. Proc Natl Acad Sci U S A 88: 6991–6995.
27. *Herr W (1984)* Nucleotide sequence of AKV murine leukemia virus. J Virol 49: 471–478.
28. O'Neill RR, Buckler CE, Theodore TS, Martin MA, Repaske R (1985) Envelope and long terminal repeat sequences of a cloned infectious NZB xenotropic murine leukemia virus. *J Virol 53: 100–106.*
29. Perryman S, Nishio J, Chesebro B (1991) Complete nucleotide sequence of Friend murine leukemia virus, strain FB29. Nucleic Acids Res 19: 6950.
30. Shinnick TM, Lerner RA, Sutcliffe JG (1981) Nucleotide sequence of Moloney murine leukaemia virus. Nature 293: 543–548.
31. Sijts EJ, Leupers CJ, Mengede EA, Loenen WA, van den Elsen PJ, et al. (1994) Cloning of the MCF1233 murine leukemia virus and identification of sequences involved in viral tropism, oncogenicity and T cell epitope formation. Virus Res 34: 339–349.
32. Antoine M, Wegmann B, Kiefer P (1998) Envelope and long terminal repeat sequences of an infectious murine leukemia virus from a human SCLC cell line: *Implications for gene transfer.* Virus Genes 17: 157–168.
33. Coffin JM, Hughes SH, Varmus HE (1997) Retroviruses. Cold Spring Harbor (New York): Cold Spring Harbor Laboratory Press. 843 p.
34. Battini JL, Heard JM, Danos O (1992) Receptor choice determinants in the envelope glycoproteins of amphotropic, xenotropic, and polytropic murine leukemia viruses. J Virol 66: 1468–1475.
35. Fass D, Davey RA, Hamson CA, Kim PS, Cunningham JM, et al. (1997) Structure of a murine leukemia virus receptor-binding glycoprotein at 2.0 angstrom resolution. Science 277: 1662–1666.
36. Tailor CS, Lavillette D, Marin M, Kabat D (2003) Cell surface receptors for gammaretroviruses. Curr Top Microbiol Immunol 281: 29–106.
37. Khan AS, Martin MA (1983) Endogenous murine leukemia proviral long terminal repeats contain a unique 190-base-pair insert. Proc Natl Acad Sci U S A 80: 2699–2703.
38. Battini JL, Rasko JE, Miller AD (1999) A human cell-surface receptor for xenotropic and polytropic murine leukemia viruses: *Possible role in G* protein–coupled signal transduction. Proc Natl Acad Sci U S A 96: 1385–1390.
39. Tailor CS, Nouri A, Lee CG, Kozak C, Kabat D (1999) Cloning and characterization of a cell surface receptor for xenotropic and polytropic murine leukemia viruses. Proc Natl Acad Sci U S A 96: 927–932.
40. Yang YL, Guo L, Xu S, Holland CA, Kitamura T, et al. (1999) Receptors for polytropic and xenotropic mouse leukaemia viruses encoded by a single gene at Rmc1. Nat Genet 21: 216–219.
41. Temin HM (1981) Structure, variation and synthesis of retrovirus long terminal repeat. *Cell 27: 1–3.*
42. Celander D, Hsu BL, Haseltine WA (1988) Regulatory elements within the murine leukemia virus enhancer regions mediate glucocorticoid responsiveness. J Virol 62: 1314–1322.
43. Speck NA, Baltimore D (1987) Six distinct nuclear factors interact with the 75-base-pair repeat of the Moloney murine leukemia virus enhancer. Mol Cell Biol 7: 1101–1110.
44. DeFranco D, Yamamoto KR (1986) Two different factors act separately or together to specify functionally distinct activities at a single transcriptional enhancer. Mol Cell Biol 6: 993–1001.
45. Miksicek R, Heber A, Schmid W, Danesch U, Posseckert G, et al. (1986) *Glucocorticoid responsiveness of the transcriptional enhancer of Moloney* murine sarcoma virus. Cell 46: 283–290.
46. Bruland T, Lavik LA, Dai HY, Dalen A (2003) A glucocorticoid response element in the LTR U3 region of Friend murine leukaemia virus variant *FIS-2 enhances virus production in vitro and is a major determinant for sex* differences in susceptibility to FIS-2 infection in vivo. J Gen Virol 84: 907–916.
47. Bruland T, Dai HY, Lavik LA, Kristiansen LI, Dalen A (2001) Gender-related differences in susceptibility, early virus dissemination and immunosuppression in mice infected with Friend murine leukaemia virus variant FIS-2. J Gen Virol 82: 1821–1827.
48. Thomas CY, Coppola MA, Holland CA, Massey AC (1990) Oncogenicity and U3 region sequences of class II recombinant MuLVs of CWD mice. Virology 176: 166–177.
49. Tomonaga K, Coffin JM (1999) Structures of endogenous nonecotropic *murine leukemia virus (MLV) long terminal repeats in wild mice:* Implication for evolution of MLVs. J Virol 73: 4327–4340.
50. Adam MA, Miller AD (1988) Identification of a signal in a murine retrovirus that is sufficient for packaging of nonretroviral RNA into virions. J Virol 62: 3802–3806.
51. Fisher J, Goff SP (1998) Mutational analysis of stem-loops in the RNA packaging signal of the Moloney murine leukemia virus. Virology 244: 133–145.
52. Berlioz C, Darlix JL (1995) An internal ribosomal entry mechanism promotes translation of murine leukemia virus gag polyprotein precursors. J Virol 69: 2214–2222.
53. Vagner S, Waysbort A, Marenda M, Gensac MC, Amalric F, et al. (1995) Alternative translation initiation of the Moloney murine leukemia virus mRNA controlled by internal ribosome entry involving the p57/PTB splicing factor. J Biol Chem 270: 20576–20583.
54. Prats AC, De Billy G, Wang P, Darlix JL (1989) CUG initiation codon used for the synthesis of a cell surface antigen coded by the murine leukemia virus. J Mol Biol 205: 363–372.
55. Fan H, Chute H, Chao E, Feuerman M (1983) Construction and characterization of Moloney murine leukemia virus mutants *unable to synthesize* glycosylated gag polyprotein. Proc Natl Acad Sci U S A 80: 5965–5969.
56. Schwartzberg P, Colicelli J, Goff SP (1983) Deletion mutants of Moloney murine leukemia virus which lack glycosylated gag protein are replication competent. J Virol 46: 538–546.
57. Chun R, Fan H (1994) Recovery of Glycosylated gag Virus from Mice Infected with a Glycosylated gag-Negative Mutant of Moloney Murine Leukemia Virus. J Biomed Sci 1: 218–223.
58. Corbin A, Prats AC, Darlix JL, Sitbon M (1994) A nonstructural gag-encoded glycoprotein precursor is necessary for efficient spreading and pathogenesis of murine leukemia viruses. J Virol 68: 3857–3867.
59. Fujisawa R, McAtee FJ, Zirbel JH, Portis JL (1997) Characterization of glycosylated Gag expressed by a neurovirulent murine leukemia virus: Identification of differences in processing in vitro and in vivo. J Virol 71: 5355–5360.
60. Munk C, Prassolov V, Rodenburg M, Kalinin V, Lohler J, et al. (2003) 10A1-MuLV but not the related amphotropic 4070A MuLV is highly neurovirulent: Importance of sequences upstream of the structural Gag coding region. Virology 313: 44–55.
61. Portis JL, Fujisawa R, McAtee FJ (1996) The glycosylated gag protein of MuLV is a determinant of neuroinvasiveness: Analysis of second site revertants of a mutant MuLV lacking expression of this protein. Virology 226: 384–392.
62. Fujisawa R, McAtee FJ, Wehrly K, Portis JL (1998) The neuroinvasiveness of a murine retrovirus is influenced by a dileucine-containing sequence in the cytoplasmic tail of glycosylated Gag. J Virol 72: 5619–5625.
63. Bracho MA, Moya A, Barrio E (1998) Contribution of Taq polymerase-induced errors to the estimation of RNA virus diversity. J Gen Virol 79 (Part 12): 2921–2928.
64. Wernert N, Seitz G, Achtstatter T (1987) Immunohistochemical inves*tigation of different cytokeratins and vimentin in the prostate from the* fetal period up to adulthood and in prostate carcinoma. Pathol Res Pract 182: 617–626.
65. Chesebro B, Britt W, Evans L, Wehrly K, Nishio J, et al. (1983) Characterization of monoclonal antibodies reactive with murine leukemia viruses: Use in analysis of strains of friend MCF and Friend ecotropic murine leukemia virus. Virology 127: 134–148.
66. Tomonaga K, Coffin JM (1998) Structure and distribution of endogenous nonecotropic murine leukemia viruses in wild mice. J Virol 72: 8289–8300.
67. Albritton LM, Tseng L, Scadden D, Cunningham JM (1989) A putative murine ecotropic retrovirus receptor gene encodes a multiple membrane-spanning protein and confers susceptibility to virus infection. Cell 57: 659–666.
68. Kim JW, Closs EI, Albritton LM, Cunningham JM (1991) Transport of cationic amino acids by the mouse ecotropic retrovirus receptor. Nature 352: 725–728.
69. Wang H, Kavanaugh MP, North RA, Kabat D (1991) Cell-surface receptor for ecotropic murine retroviruses is a basic amino-acid transporter. Nature 352: 729–731.
70. *Gifford R, Tristem M (2003) The evolution, distribution and diversity of* endogenous retroviruses. Virus Genes 26: 291–315.
71. Tlsty TD, Hein PW (2001) Know thy neighbor: Stromal cells can contribute oncogenic signals. Curr Opin Genet Dev 11: 54–59.
72. Bhowmick NA, Neilson EG, Moses HL (2004) Stromal fibroblasts in cancer initiation and progression. Nature 432: 332–337.
73. Olumi AF, Grossfeld GD, Hayward SW, Carroll PR, Tlsty TD, et al. (1999) Carcinoma-associated fibroblasts direct tumor progression of initiated human prostatic epithelium. Cancer Res 59: 5002–5011.
74. Eisen MB, Spellman PT, Brown PO, Botstein D (1998) Cluster analysis and display of genome-wide expression patterns. Proc Natl Acad Sci U S A 95: 14863–14868.
75. Saldanha AJ (2004) Java Treeview—Extensible visualization of microarray data. Bioinformatics 20: 3246–3248.
76. Gordon D, Abajian C, Green P (1998) Consed: A graphical tool for sequence finishing. Genome Res 8: 195–202.
77. Stoye JP, Coffin JM (1987) The four classes of endogenous murine leukemia virus: Structural relationships and potential for recombination. J Virol 61: 2659–2669.
78. *Thompson JD, Gibson TJ, Plewniak F, Jeanmougin F, Higgins DG (1997)* The CLUSTAL_X windows interface: Flexible strategies for multiple sequence alignment aided by quality analysis tools. Nucleic Acids Res 25: 4876–4882.
79. Jeanmougin F, Thompson JD, Gouy M, Higgins DG, Gibson TJ (1998) Multiple sequence alignment with Clustal X. Trends Biochem Sci 23: 403–405.
80. *Kimura M (1980) A simple method for estimating evolutionary rates of base* substitutions through comparative studies of nucleotide sequences. J Mol Evol 16: 111–120.
81. Bray N, Dubchak I, Pachter L (2003) AVID: A global alignment program. Genome Res 13: 97–102.
82. Frazer KA, Pachter L, Poliakov A, Rubin EM, Dubchak I (2004) VISTA: Computational tools for comparative genomics. Nucleic Acids Res 32: W273–W279.

Virus in Prostate Tumors with R462Q *RNASEL*